Supporting Information

Surfacial Enriched Ru onto Octahedral CeO_2 with Strong Electronic Interactions as Efficient Electrocatalyst for Hydrogen Generation in Alkaline Freshwater/seawater

Jing Li[a], Ruotong Guo[a], Xingchao Zang[a], Yue Wang[a], Hongdong Li[a], Weiping Xiao[b], Liantao Xin[a], Yingxia Zong[a], Guangying Fu[c], Zexing Wu[a, *], Lei Wang[a, *]

a. Key Laboratory of Eco-chemical Engineering, Ministry of Education, International Science and Technology Cooperation Base of Eco-chemical Engineering and Green Manufacturing, College of Chemistry and Molecular Engineering, Qingdao University of Science & Technology 53 Zhengzhou Road, 266042, Qingdao, P. R. China E-mail: splswzx@qust.edu.cn; inorchemwl@126.com.

b. College of Science, Nanjing Forestry University, Nanjing, 210037, P. R. China.

c. Key Laboratory of Photoelectric Conversion and Utilization of Solar Energy, Qingdao Institute of Bioenergy and Bioprocess Technology, Chinese Academy of Sciences, CN-266101 Qingdao, China.

*Corresponding authors

1. Experimental Section

1.1 Chemicals and Materials

Cerium nitrate hexahydrate ($Ce(NO_3)_3 \cdot 6H_2O$), sodium phosphate (Na_3PO_4), ruthenium (III) chloride anhydrous ($RuCl_3$), hydrogen peroxide aqueous solution (30 % H_2O_2), potassium hydroxide (KOH), sulfuric acid (H_2SO_4), commercial Pt/C (20 *wt* % platinum on carbon black) and ruthenium dioxide (RuO_2).

1.2 Synthesis of CeO_2

0.87 g $Ce(NO_3)_3 \cdot 6H_2O$ and 0.0076 g Na_3PO_4 were added into a beaker containing 80 mL of deionized water and stirred for 30 minutes at room temperature. Then, the above solution was added to the Teflon-lined autoclave and placed in an oven at 170 °C for 600 min. After cooling to room temperature, the solution was centrifuged with deionized water and ethanol several times and put it into the oven for drying. The dried powder was oxidized in a tune furnace at 350 °C for 3 hours to obtain white CeO_2 powder.[1]

1.3 Synthesis of Ru/CeO_2-H_2O_2

10 mg of anhydrous $RuCl_3$ and 20 mg CeO_2 were fully ground to obtain the black powder, and then put it into the porcelain boat and added 10 μL of H_2O_2 reaction for one minute. Then, added 20 mL deionized water and evaporated it at 80 °C with stirring to obtain black Ru/CeO_2-H_2O_2.

1.4 Synthesis of CeO_2-H_2O_2

The synthesis of CeO_2-H_2O_2 was identical to the Ru/CeO_2-H_2O_2 without the addition of $RuCl_3$.

2. Physical Characterization

Physical characterizations of the involved catalysts were performed by scanning electron microscope (SEM) (Regulus 8100) and transmission electron microscopy (TEM) (JEM-F200). X-ray diffraction (XRD) (Japan Rigaku Ultima IV) and X-ray photoelectron spectroscopy (XPS) (America Thermo Scientific K-Alpha) were used to determine the crystal structure and chemical composition. Electron paramagnetic resonance (EPR) (BRUKE EMXPLUS) can be used to qualitatively and quantitatively detect oxygen vacancies in catalysts. Raman spectroscopy (D-MAX 2500/PC) can analyze the structural information of the catalysts. Inductively coupled plasma optical emission spectrometer (ICP-OES) (Hitachi U4150) analyzes the amount of Ru in the catalyst.

3. Electrochemical Measurements

All electrochemical measurements were conducted using a typical three-electrode setup in 1 M KOH and 0.5 M H_2SO_4 with a reversible hydrogen electrode (RHE), glassy carbon electrode and carbon rod as the reference electrode, working electrode, and counter electrode, respectively, at room temperature. In 1 M KOH + seawater, glassy carbon electrode, Ag/AgCl electrodes and graphite rods were used as working electrode, reference electrode, and counter electrode, respectively. All the potentials were transformed to the RHE according to the following equation: $E_{RHE} = E_{Ag/AgCl} + 0.0592\ pH + 0.197$. For ink preparation, 5 mg of catalyst and 1mg of carbon black were added to 1 mL Nafion solution and sonicated for 30 minutes. Then, the 20 μL prepared ink was applied to the glassy carbon electrode for testing. Linear sweep voltammetry (LSV) was collected with scanning rate of 5 mV s^{-1} with 95% IR compensation. Electrochemical impedance spectroscopy (EIS) measurements were carried out in frequency ranges from 100 kHz to 0.01 Hz with an amplitude of 5 mV. Multi-step chronopotentiometry, multi-step chronoamperometry and chronoamperometry were performed to study the stability of the prepared catalysts.

3.1 Cyclic voltammetry (CV) Measurements

CV was performed with different scan rates (20-120 mV s^{-1}) in the non-Faraday interval.

3.2 Mass activity computation

Mass activity = Current (mA) / $m_{Ru\ (Pt)}$

Current is taken from linear sweep voltammetry curves at an overpotential of 100 mV, and $m_{Ru(Pt)}$ is the mass of Ru(Pt) on the working electrode.

3.3 Turnover frequency calculation (TOF)

TOF is a familiar evaluation criterion of catalysts, which is identified as the number of reactants of the electrocatalytic active sites per area to convert to the expected product per time.[2]

Total hydrogen turnovers

$$= \left(|j|\frac{\text{mA}}{\text{cm}^2}\right)\left(\frac{\frac{1\text{C}}{\text{s}}}{1000\ \text{mA}}\right)\left(\frac{1\ \text{mol e}^-}{96485.3\ \text{C}}\right)\left(\frac{1\ \text{mol}}{2\ \text{mol e}^-}\right)\left(\frac{6.022\times10^{23}\ \text{molecules H}_2}{1\ \text{mol H}_2}\right)$$

$$= 3.12\times10^{15}\frac{\text{H}_2/\text{s}}{\text{cm}^2}\text{per}\frac{\text{mA}}{\text{cm}^2}$$

Ru/CeO_2 - H_2O_2 (active sites) 10 mV

$$= \left(\frac{\text{catalyst loading per geometric area } \times \left(\frac{\text{g}}{\text{cm}^2}\right) \times \text{Ru } wt\%}{\text{Ru M}_\text{W}\left(\frac{\text{g}}{\text{mol}}\right)}\right)\left(\frac{6.022\times10^{23}\text{Ru atomes}}{1\ \text{mol Ru}}\right)$$

$$= \left(\frac{0.509\times\frac{10^{-3}\text{g}}{\text{cm}^2}\times 12.40\ wt\%}{101.1}\right)\left(\frac{6.022\times10^{23}\text{Ru atomes}}{1\ \text{mol Ru}}\right)$$

$$= 3.76\times10^{17}\ \text{Ru sites per cm}^2$$

$$\text{TOF} = \left(\frac{3.12\times10^{15}}{3.76\times10^{17}}\times|j|\right) = 8.30\times10^{-3}\times|-2.06| = 0.017\ Ru\ sites\ per\ cm^2$$

Ru/CeO_2 - H_2O_2 (active sites) 50 mV

$$\text{TOF} = \left(\frac{3.12\times10^{15}}{3.76\times10^{17}}\times|j|\right) = 8.30\times10^{-3}\times|-15.56| = 0.13\ Ru\ sites\ per\ cm^2$$

Ru/CeO_2 - H_2O_2 (active sites) 100 mV

$$\text{TOF} = \left(\frac{3.12\times10^{15}}{3.76\times10^{17}}\times|j|\right) = 8.30\times10^{-3}\times|-51.92| = 0.43\ \text{Ru sites per cm}^2$$

Pt/C (active sites)10 mV

$$= (|j|\frac{\text{mA}}{\text{cm}^2})(\frac{\frac{1\text{C}}{\text{s}}}{1000\text{ mA}})(\frac{1\text{ mol e}^-}{96485.3\text{ C}})(\frac{1\text{ mol}}{2\text{ mol e}^-})(\frac{6.022\times10^{23}\text{ molecules H}_2}{1\text{ mol H}_2})$$

$$= 3.12\times10^{15}\frac{\text{H}_2\text{/s}}{\text{cm}^2}\text{per}\frac{\text{mA}}{\text{cm}^2}$$

$$= \left(\frac{\text{catalyst loading per geometric area }\times\left(\frac{\text{g}}{\text{cm}^2}\right)\times\text{Pt wt\%}}{\text{Pt M}_\text{W}\left(\frac{\text{g}}{\text{mol}}\right)}\right)\left(\frac{6.022\times10^{23}\text{Pt atomes}}{1\text{ mol Pt}}\right)$$

$$= \left(\frac{0.509\times\frac{10^{-3}\text{g}}{\text{cm}^2}\times20\text{ wt\%}}{195}\right)\left(\frac{6.022\times10^{23}\text{Pt atomes}}{1\text{ mol Pt}}\right)$$

$$= 3.14\times10^{17}\text{ Pt sites per cm}^2$$

$$\text{TOF} = \left(\frac{3.12\times10^{15}}{3.15\times10^{17}}\times|j|\right) = 9.90\times10^{-3}\times|-0.82| = 0.0082\text{ Pt sites per cm}^2$$

Pt/C (active sites) 50 mV

$$\text{TOF} = \left(\frac{3.12\times10^{15}}{3.15\times10^{17}}\times|j|\right) = 9.90\times10^{-3}\times|-7.85| = 0.077\text{ Pt sites per cm}^2$$

Pt/C (active sites) 100 mV

$$\text{TOF} = \left(\frac{3.12\times10^{15}}{3.15\times10^{17}}\times|j|\right) = 9.90\times10^{-3}\times|-23.99| = 0.24\text{ Pt sites per cm}^2$$

Ru/CeO_2 - H_2O_2 (active sites) 10 mV = 0.017 Ru sites per cm^2

Ru/CeO_2 - H_2O_2(active sites) 50 mV = 0.13 Ru sites per cm^2

Ru/CeO_2 - H_2O_2 (active sites) 100 mV = 0.43 Ru sites per cm^2

Pt/C (active sites) 10 mV= 0.0082 Pt sites per cm^2

Pt/C (active sites) 50 mV = 0.080 Pt sites per cm^2

Pt/C (active sites) 100 mV = 0.24 Pt sites per cm^2

1 M KOH: When the overpotential is 10 mV, 50 mV, 100 mV, the current density of Ru/CeO_2-H_2O_2 are 2.06 mA cm^{-2}, 15.56 mA cm^{-2}, 51.92 mA cm^{-2}, TOF=0.017 H_2 s^{-1}, 0.13 H_2 s^{-1}, 0.43 H_2 s^{-1}. Similarly, the current density of Pt/C at 10 mV, 50 mV, 100 mV are 0.82 mA cm^{-2}, 7.85 mA cm^{-2}, 23.99 mA cm^{-2} and TOF = 0.0082 H_2 s^{-1}, 0.080 H_2 s^{-1} and 0.24 H_2 s^{-1}.

4. DFT Calculations

All density functional theory calculations were performed by Vienna ab initio simulation package (VASP).[3] The Perdew-Burke-Ernzerhof (PBE)[4] functional was employed to treat the exchange-correlation interactions. The plane-wave basis set with a kinetic energy cutoff of 400 eV, the energy convergence criterion of 10^{-4} eV, the force convergence criterion of 0.02 eV $Å^{-1}$, and a (1×1×1) Monkhorst-Pack k-point sampling was employed for structure relaxation. A sufficiently large vacuum gap (> 12 Å) was employed to prevent the interaction between neighboring periodic structures. H_2 and H_2O were calculated in boxes of 20 Å×20 Å×20 Å with the gamma point only. The free energy diagrams for HER were calculated with reference to the computational hydrogen electrode.[5] The free energy of gas phase and adsorbed species can be obtained from the following equation:

$\Delta G=\Delta E_{DFT} + \Delta ZPE - T\Delta S$

where T was set as 298.15 K. ΔZPE and TΔS was the change in the zero point energy and entropy.

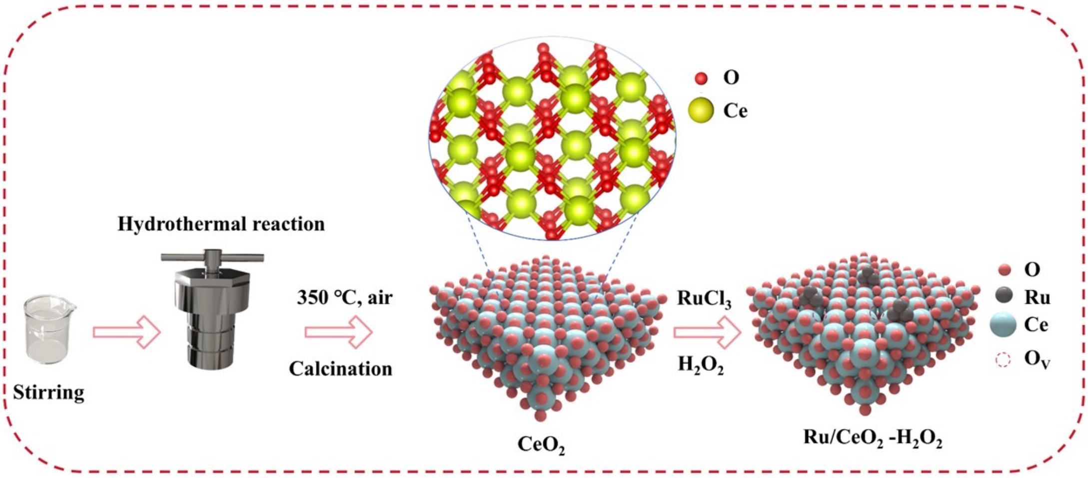

Figure S1. Schematic of the synthesis procedure for CeO_2 and octahedral Ru/CeO_2-H_2O_2.

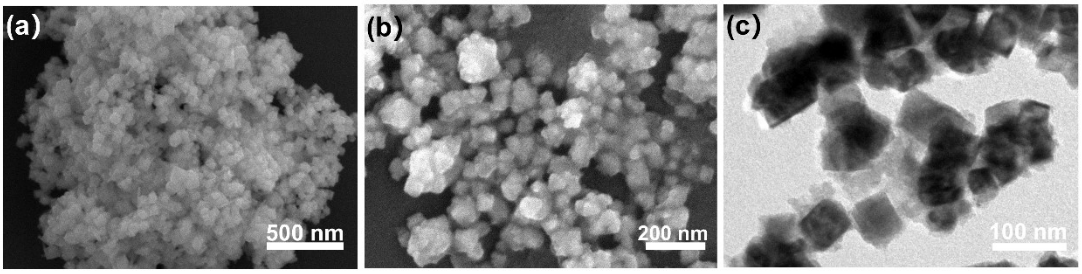

Figure S2. SEM images of (a) CeO_2-H_2O_2 and (b) Ru/CeO_2-H_2O_2. (c) TEM image of Ru/CeO_2-H_2O_2.

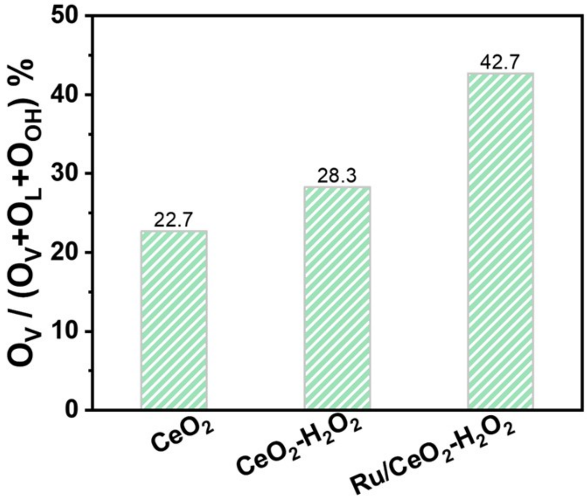

Figure S3. The oxygen vacancy content in various catalysts.

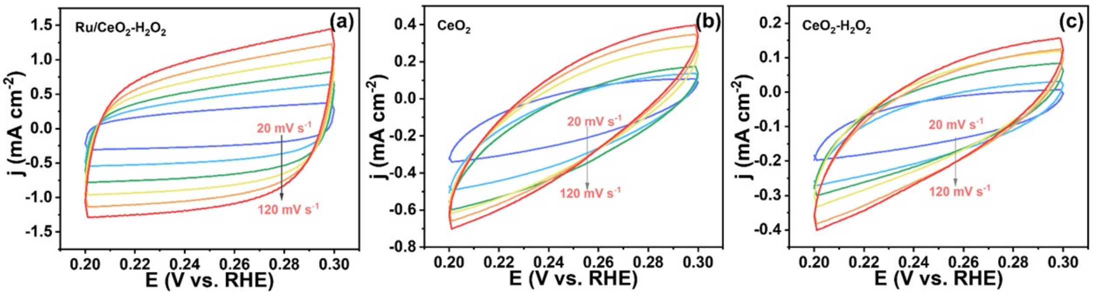

Figure S4. The CV plots with different scan rates of (a) Ru/CeO_2-H_2O_2, (b) CeO_2 and (c) CeO_2-H_2O_2 in 1 M KOH.

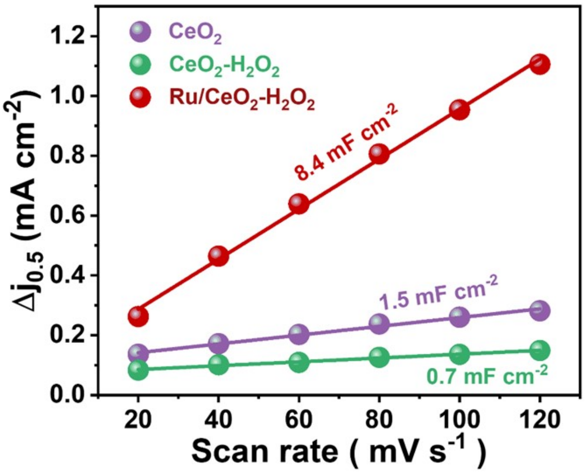

Figure S5. The electrochemical double-layer capacitance (C_{dl}) of Ru/CeO_2-H_2O_2, CeO_2-H_2O and CeO_2.

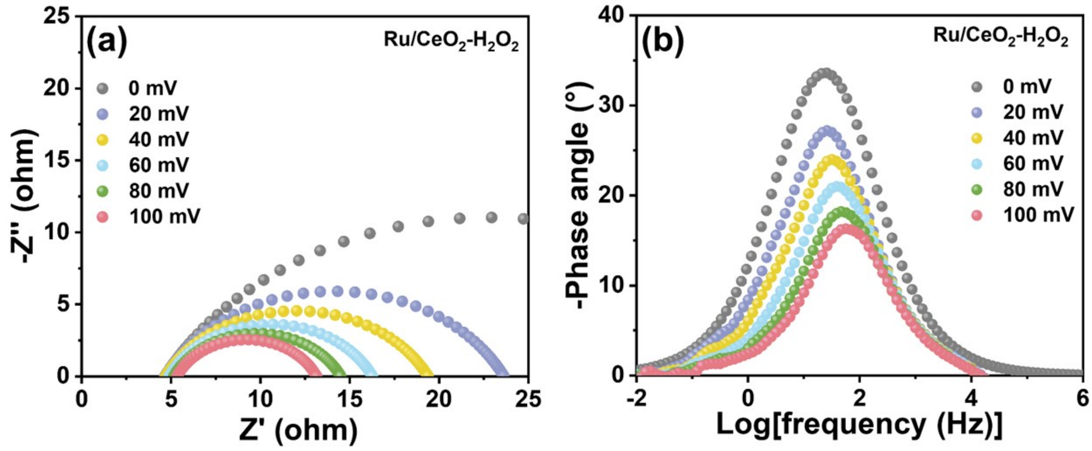

Figure S6. (a) Nyquist plots and (b) Bode plots of Ru/CeO_2-H_2O_2 at different overpotentials.

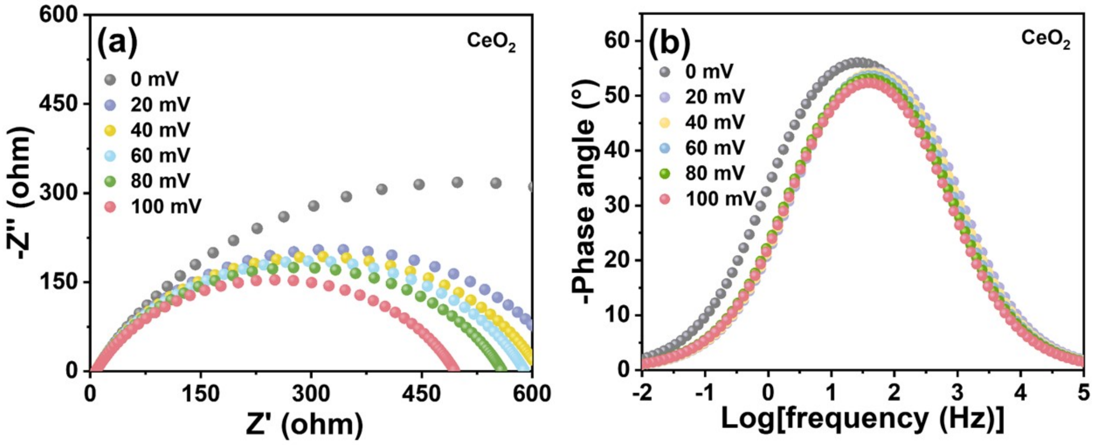

Figure S7. (a) Nyquist plots and (b) Bode plots of CeO_2 at different overpotentials.

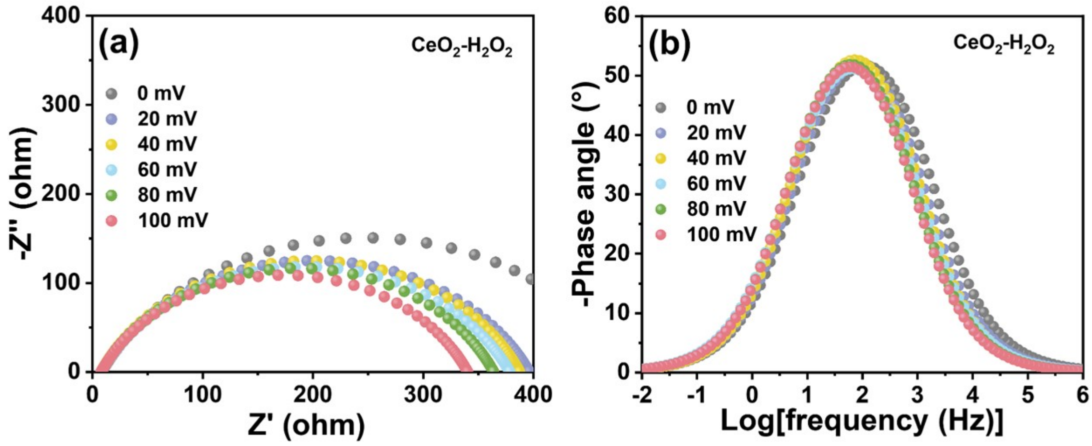

Figure S8. (a) Nyquist plots and (b) Bode plots of CeO_2-H_2O_2 at different overpotentials.

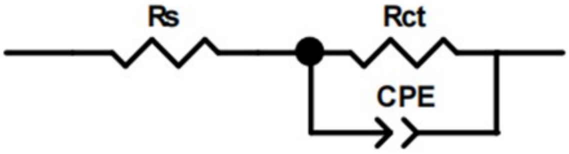

Figure S9. The equivalent circuit for Ru/CeO_2-H_2O, CeO_2 and CeO_2-H_2O_2.

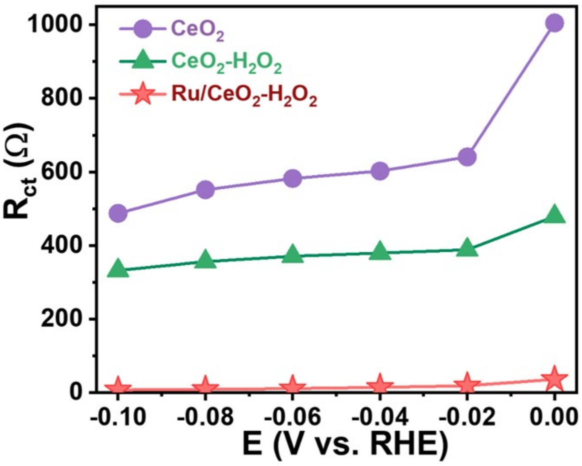

Figure S10. Charge transfer resistance (R$_{ct}$) at different potentials.

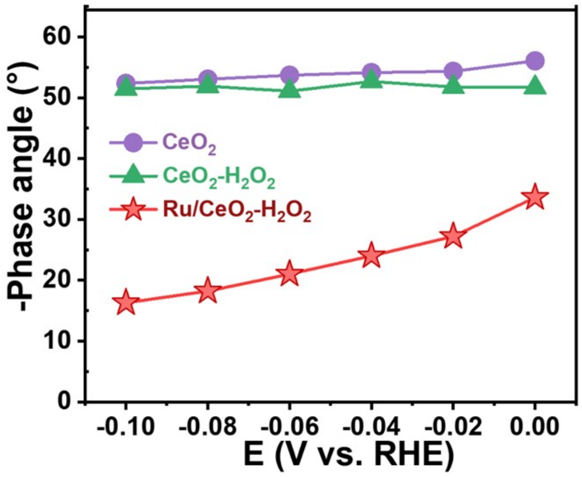

Figure S11. Phase peak angles of Ru/CeO_2-H_2O_2, CeO_2, CeO_2-H_2O_2 at different potentials.

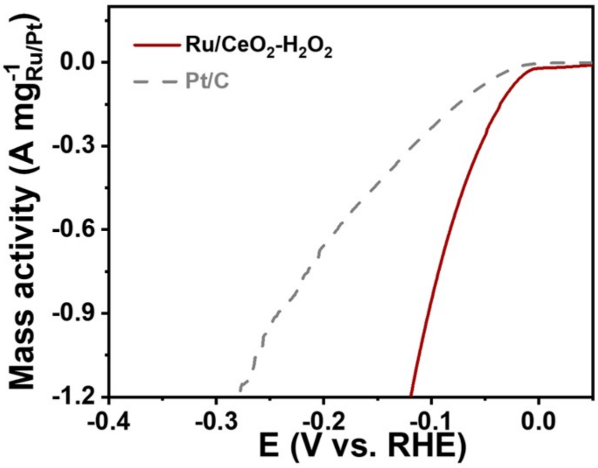

Figure S12. Polarization curves normalized by mass contents of Ru or Pt in Ru/CeO$_2$-H$_2$O$_2$ and Pt/C.

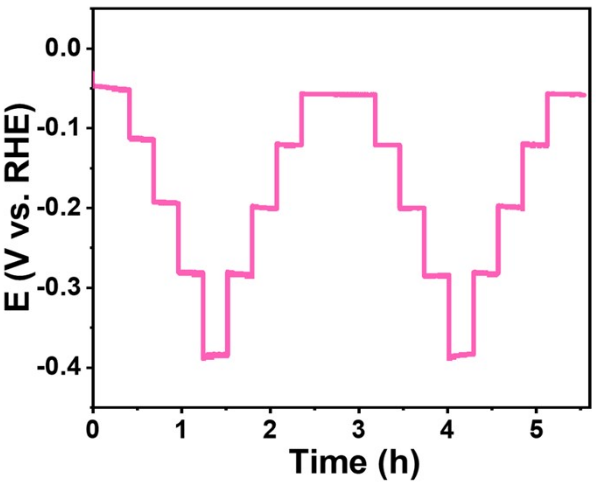

Figure S13. Multiple-step chronopotentiometric measurement in 1 M KOH.

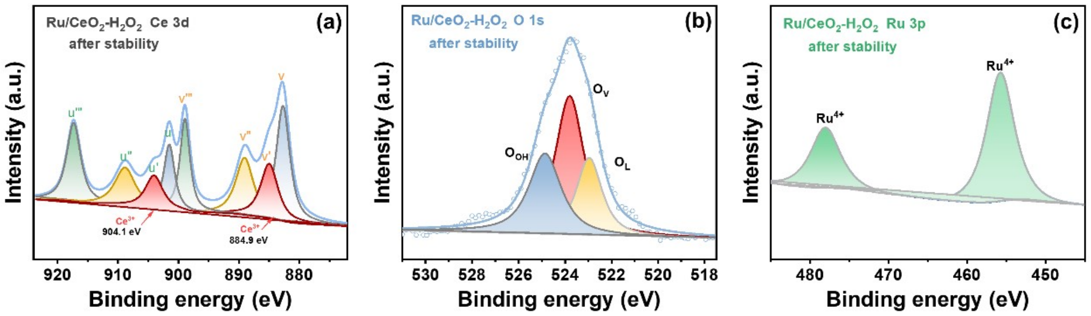

Figure S14. XPS spectra of (a) Ce 3d, (b) O 1s and (c) Ru 3p in Ru/CeO_2-H_2O_2 after stability.

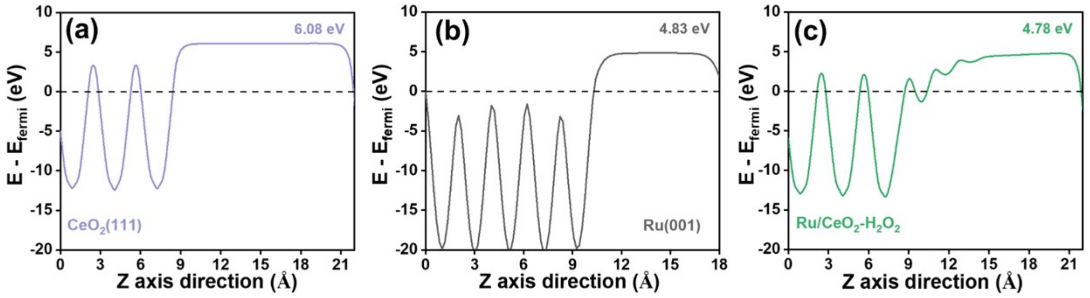

Figure S15. The computed work function values for the CeO_2 (111), Ru (001), Ru/CeO_2-H_2O_2.

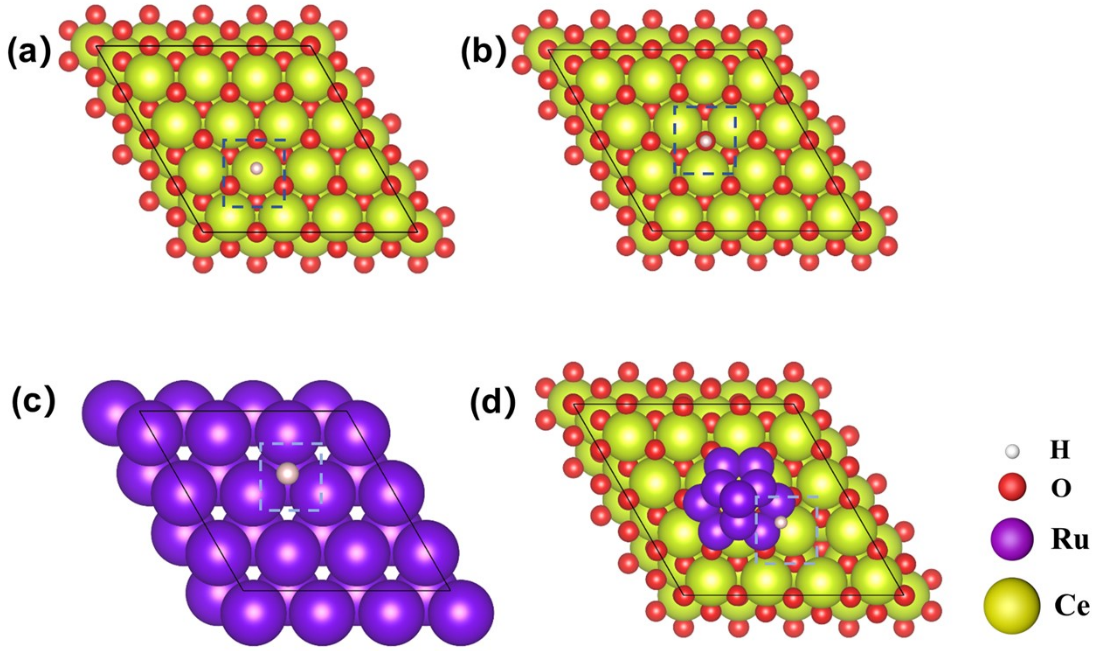

Figure S16. H adsorbed at the (a) Ce site, (b) O site, (c) Ru (001) site and (d) interface of Ru/CeO_2 (111)-Ov.

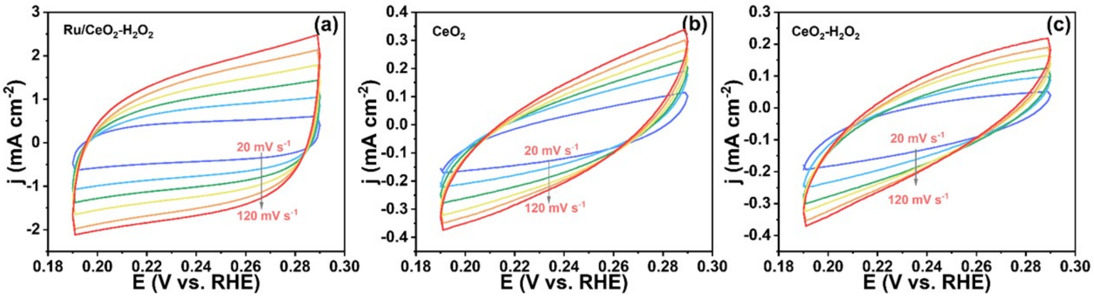

Figure S17. The CV plots with different scan rates of (a) Ru/CeO$_2$-H$_2$O$_2$, (b) CeO$_2$ and (c) CeO$_2$-H$_2$O$_2$ in 1 M KOH + seawater.

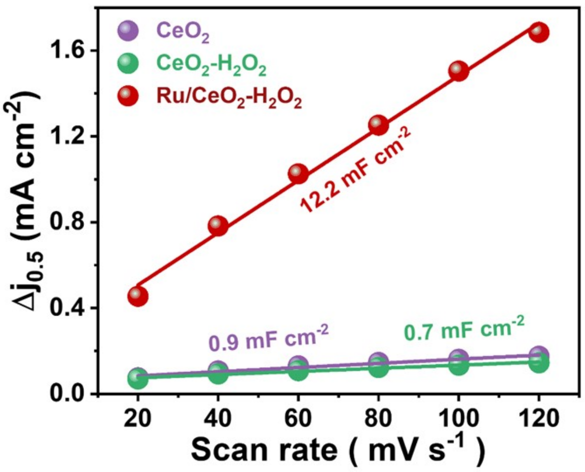

Figure S18. The C_{dl} of Ru/CeO$_2$-H$_2$O$_2$, CeO$_2$-H$_2$O and CeO$_2$ in 1 M KOH + seawater.

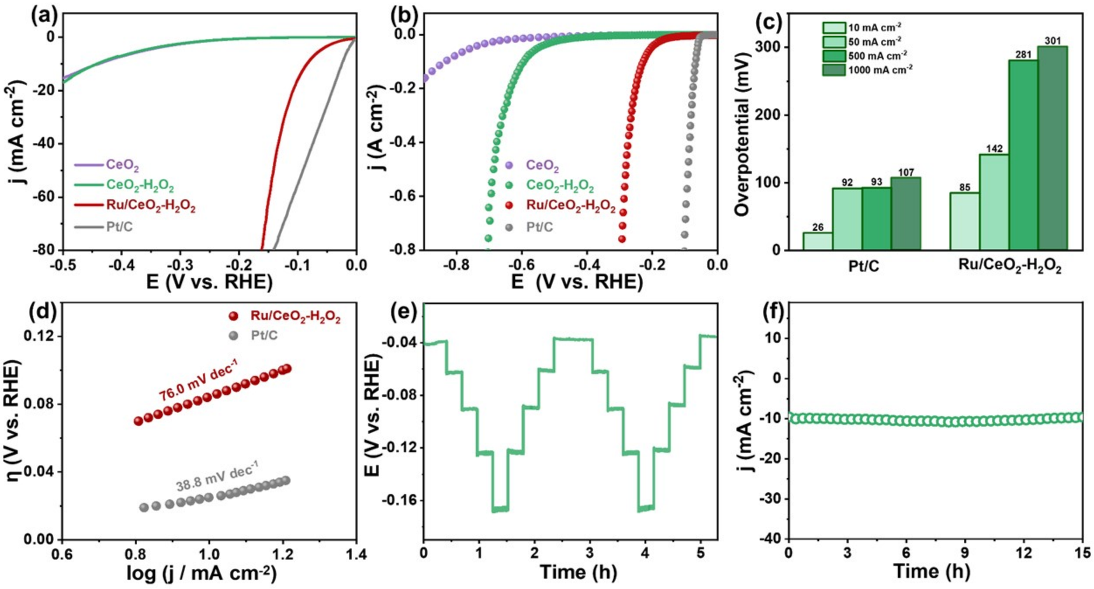

Figure S19. HER performance of Ru/CeO$_2$-H$_2$O$_2$ in 0.5 M H_2SO_4. Polarization curves of Pt/C, Ru/CeO$_2$-H$_2$O$_2$, CeO$_2$-H$_2$O$_2$ and CeO$_2$ at (a) low and (b) high current densities. (c) Comparison of overpotentials of Ru/CeO$_2$-H$_2$O$_2$ and Pt/C at different current densities. (d) Corresponding Tafel slopes. (e) Multiple-step chronopotentiometric measurement. (f) Chronoamperometric measurement of Ru/CeO$_2$-H$_2$O$_2$ in 0.5 M H_2SO_4.

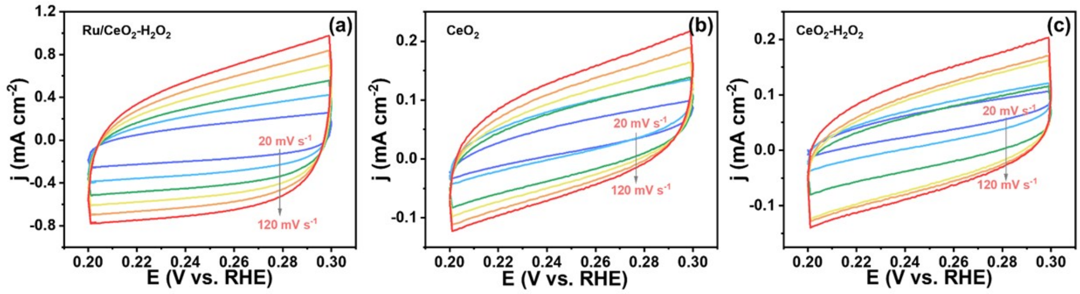

Figure S20. The CV plots with different scan rates of Ru/CeO$_2$-H$_2$O$_2$, CeO$_2$ and CeO$_2$-H$_2$O$_2$ in 0.5 M H$_2$SO$_4$.

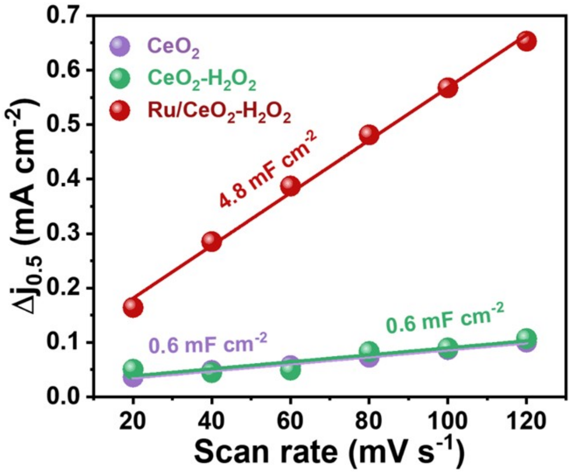

Figure S21. The C_{dl} of Ru/CeO_2-H_2O_2, CeO_2-H_2O and CeO_2 in 0.5 M H_2SO_4.

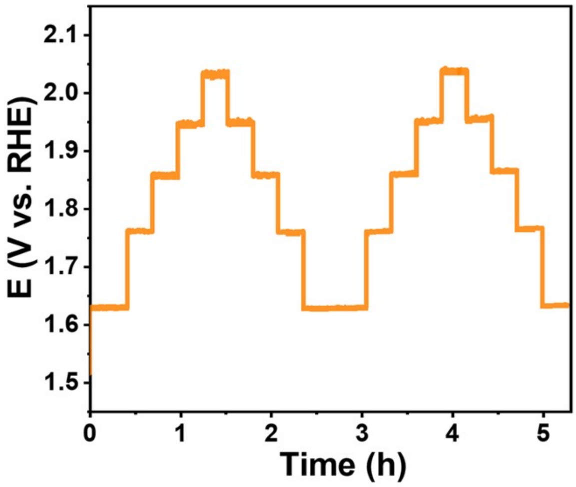

Figure S22. Multi-step chronopotentiometric measurement for overall water splitting (OWS).

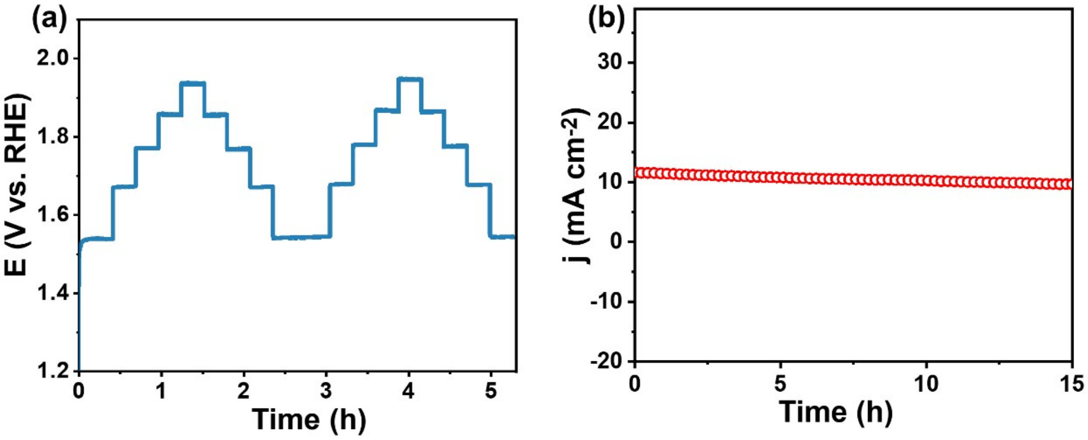

Figure S23. (a) Multi-step chronopotentiometric measurement and (b) long-term stability test for overall seawater splitting.

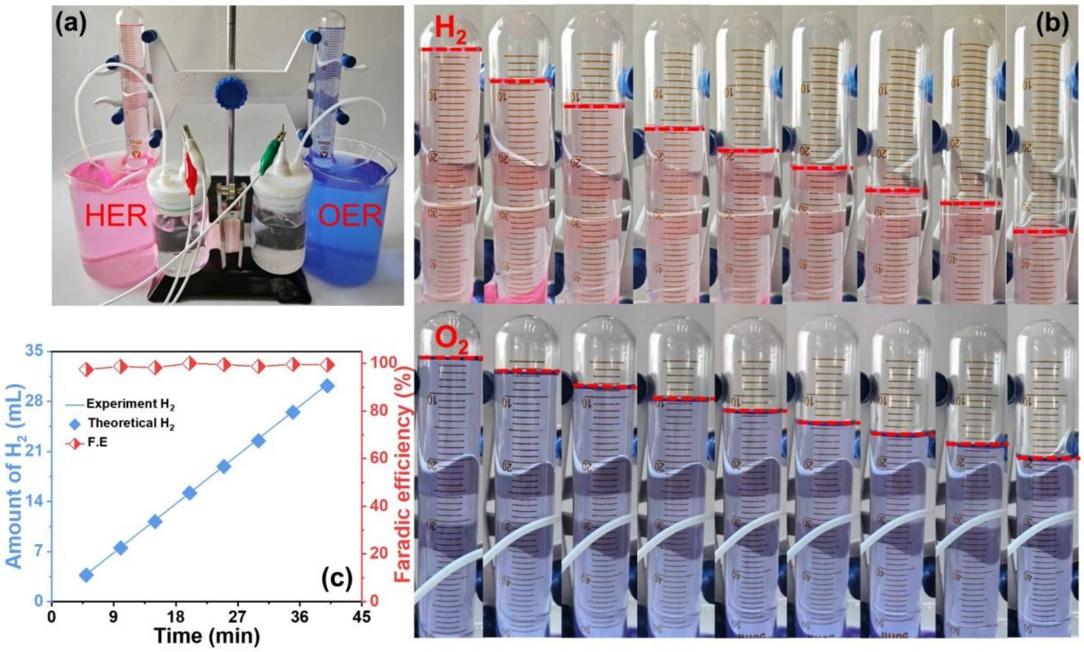

Figure S24. (a) Optical photograph of $RuO_2||Ru/CeO_2-H_2O_2$ two-electrode device for OWS. (b) Optical photograph of drainage method collecting gas system. (c) Faradic efficiencies of $RuO_2||Ru/CeO_2-H_2O_2$ electrolyzer under 100 mAcm^{-2} in 1 M KOH solution.

Table S1. The ICP-OES (Ru) of Ru/CeO_2-H_2O_2.

ICP-OES (Ru)	*wt* %
Ru/CeO_2-H_2O_2	12.40

Table S2. Comparison of the HER activity of the Ru/CeO_2-H_2O_2 with other previously reported electrocatalysts in 1 M KOH.

Catalysts	Overpotential (mV)@ 10 mA cm^{-2}	Tafel slope (mV dec^{-1})	References
Ru/CeO_2-H_2O_2	37	36.7	This work
Ru-H_2O/CC	44	91	6
Ru-NiCoP/NF	44	45.4	7
Ru/OG	48	32.4	8
Ru/Co_4N-CoF_2	53	144.1	9
Ru SAs-Ni_2P	57	75	10
N-Ru-1/C	67	125	11
N-Ru/Sb_2S_3	72	193	12
RuCu NPs/C	111	73.1	13

Table S3. Comparison of the HER activity of the Ru/CeO_2-H_2O_2 with other previously reported electrocatalysts under 1 M KOH + seawater.

Catalysts	Overpotential (mV)@ 10mA cm^{-2}	References
Ru/CeO_2-H_2O_2	47	This work
Mo-Ru/CNTs	45	14
BPed-Ru-Gr	51	15
Ru_{22}NiMoP/NF	52	16
Ru_{1+NPs}/N-C	58	17
Co@RuCO-3	59	18
Ru/NC	72	19
Ru-Gr	82	15
Ru/BC	97	19
Ru/CNT	107	20

Reference:

1 H. Huang, Q. Dai and X. Wang, Morphology effect of Ru/CeO_2 catalysts for the catalytic combustion of chlorobenzene, *Appl. Catal. B Environ. Energy*, 2014, **158-159**, 96-105.

2 M. Wang, W. Fu, L. Du, Y. Wei, P. Rao, L. Wei, X. Zhao, Y. Wang and S. Sun, Surface engineering by doping manganese into cobalt phosphide towards highly efficient bifunctional HER and OER electrocatalysis, *Appl. Surf. Sci.*, 2020, **515**.

3 G. Kresse and J. Furthmüller, Efficient iterative schemes for ab initio total-energy calculations using a plane-wave basis set, *Phys. Rev. B*, 1996, **54**, 11169-11186.

4 J. P. Perdew, K. Burke and M. Ernzerhof, Generalized Gradient Approximation Made Simple, *Phys. Rev. Lett.*, 1996, **77**, 3865-3868.

5 J. K. Nørskov, J. Rossmeisl, A. Logadottir, L. Lindqvist, J. R. Kitchin, T. Bligaard and H. Jónsson, Origin of the Overpotential for Oxygen Reduction at a Fuel-Cell Cathode, *J. Phys. Chem. B*, 2004, **108**, 17886-17892.

6 D. Chen, R. Lu, Z. Pu, J. Zhu, H.-W. Li, F. Liu, S. Hu, X. Luo, J. Wu, Y. Zhao and S. Mu, Ru-doped 3D flower-like bimetallic phosphide with a climbing effect on overall water splitting, *Appl. Catal. B Environ. Energy*, 2020, **279**, 119396.

7 M. You, X. Du, X. Hou, Z. Wang, Y. Zhou, H. Ji, L. Zhang, Z. Zhang, S. Yi and D. Chen, In-situ growth of ruthenium-based nanostructure on carbon cloth for superior electrocatalytic activity towards HER and OER, *Appl. Catal. B Environ. Energy*, 2022, **317**, 121729.

8 P. Su, W. Pei, X. Wang, Y. Ma, Q. Jiang, J. Liang, S. Zhou, J. Zhao, J. Liu and G. Q. Lu, Exceptional Electrochemical HER Performance with Enhanced Electron Transfer between Ru Nanoparticles and Single Atoms Dispersed on a Carbon Substrate, *Angew. Chem. Int. Ed.*, 2021, **60**, 16044-16050.

9 S. Zhou, H. Jang, Q. Qin, Z. Li, M. Gyu Kim, X. Ji, X. Liu and J. Cho, Ru atom-modified Co_4N-CoF_2 heterojunction catalyst for high-performance alkaline hydrogen evolution, *Chem. Eng. J.*, 2021, **414**, 128865.

10 K. Wu, K. Sun, S. Liu, W.-C. Cheong, Z. Chen, C. Zhang, Y. Pan, Y. Cheng, Z. Zhuang, X. Wei, Y. Wang, L. Zheng, Q. Zhang, D. Wang, Q. Peng, C. Chen and Y. Li, Atomically dispersed Ni-Ru-P interface sites for high-efficiency pH-universal electrocatalysis of hydrogen evolution, *Nano Energy*, 2021, **80**, 105467.

11 Y. Zhao, X. Wang, Z. Li, P. Zhao, C. Tao, G. Cheng and W. Luo, Enhanced catalytic activity of Ru through N modification toward alkaline hydrogen electrocatalysis, *Chin. Chem. Lett.*, 2022, **33**, 1065-1069.

12 A. Maiti and S. K. Srivastava, N, Ru Codoped Pellet Drum Bundle-Like Sb_2S_3: An Efficient Hydrogen Evolution Reaction and Hydrogen Oxidation Reaction Electrocatalyst in Alkaline Medium, *ACS Appl. Mater. Interfaces*, 2020, **12**, 7057-7070.

13 Q. Yao, B. Huang, N. Zhang, M. Sun, Q. Shao and X. Huang, Channel-Rich RuCu Nanosheets for pH-Universal Overall Water Splitting Electrocatalysis, *Angew. Chem. Int. Ed.*, 2019, **58**, 13983-13988.

14 J. Sun, Z. Zhao, Z. Li, Z. Zhang, R. Zhang and X. Meng, Ultrafast carbothermal shocking fabrication of cation vacancy-rich Mo doped Ru nanoparticles on carbon nanotubes for high-performance water/seawater electrolysis, *J. Mater. Chem. A*, 2023, **11**, 22430-22440.

15 H. Yang, X. Wang, S. Xia, S. Zhang, R. Zhang, X. Li, X. F. Yu, X. Zhang and L. Bai, Black Phosphorus Modulated Ru Electrocatalyst for Highly Efficient and Durable Seawater Splitting, *Adv. Energy Mater.*, 2023, **13**, 2302727.

16 H. K. Sadhanala, A. Gupta and A. Gedanken, A bifunctional electrocatalyst for alkaline seawater splitting using ruthenium doped nickel molybdenum phosphide nanosheets, *Sustain. Energy Fuels*, 2023, **7**, 4677-4686.

17 S. Wang, M. Wang, Z. Liu, S. Liu, Y. Chen, M. Li, H. Zhang, Q. Wu, J. Guo, X. Feng, Z. Chen and Y. Pan, Synergetic Function of the Single-Atom Ru-N_4 Site and Ru Nanoparticles for Hydrogen Production in a Wide pH Range and Seawater Electrolysis, *ACS Appl. Mater. Interfaces*, 2022, **14**, 15250-15258.

18 H. Huang, H. Jung, C.-Y. Park, S. Kim, A. Lee, H. Jun, J. Choi, J. W. Han and J. Lee, Surface conversion derived core-shell nanostructures of Co particles@RuCo alloy for superior hydrogen evolution in alkali and seawater, *Appl. Catal. B Environ. Energy*, 2022, **315**, 121554.

19 B. Jiang, Z. Wang, H. Zhao, X. Wang, X. Mao, A. Huang, X. Zhou, K. Yin, K. Sheng and J. Wang, Ru nanoclusters anchored on boron- and nitrogen-doped carbon for a highly efficient hydrogen evolution reaction in alkaline seawater, *Nanoscale*, 2023, **15**, 19703-19708.

20 H. Lv, W. Guo, M. Chen, H. Zhou and Y. Wu, Rational construction of thermally stable single atom catalysts: From atomic structure to practical applications, *Chin. J. Catal.*, 2022, **43**, 71-91.